Journal of Applied Mathematics and Physics, 2025, 13(2), 490-505
https://www.scirp.org/journal/jamp
ISSN Online: 2327-4379
ISSN Print: 2327-4352

Mathematical Model of the Tapered Cantilever Beam Based on the Geometrically Exact Beam Theory

Yumei Luo[1], Yundong Li[1,2*], Linyan Li[1], Zhongxiang Li[1]

[1]School of Mathematics and Statistics, Sichuan University of Science and Engineering, Zigong, China
[2]South Sichuan Center for Applied Mathematics, Sichuan University of Science and Engineering, Zigong, China
Email: *lyd1114@126.com

How to cite this paper: Luo, Y.M., Li, Y.D., Li, L.Y. and Li, Z.X. (2025) Mathematical Model of the Tapered Cantilever Beam Based on the Geometrically Exact Beam Theory. *Journal of Applied Mathematics and Physics*, **13**, 490-505.
https://doi.org/10.4236/jamp.2025.132027

Received: January 18, 2025
Accepted: February 17, 2025
Published: February 20, 2025

Abstract

Based on the geometrically exact beam theory, the mathematical model of the tapered cantilever beam is built, and analysis of the structures under load is completed. With the stress-strain relationship of geometrically exact beam theory, and the principle of virtual displacement and D'Alembert principle, the virtual work balance equation of the tapered cantilever beam element is derived. The internal force, external force, and inertial force virtual work of the beam element is discretized by weak form quadrature element method. The numerical results show the variation of the natural frequency of the beam with the taper when the tapered cantilever beam is not subjected to the load and the free end is subjected to the concentrated load and bending moment.

Keywords

Geometrically Exact Beam Theory, The Tapered Cantilever Beam, Natural Frequency

1. Introduction

The tapered cantilever beam, renowned for its straightforward design and exceptional mechanical properties in terms of mass and strength distribution, holds immense potential for widespread application in the engineering domain [1]-[3]. However, in practical work, the mechanical behavior of the tapered cantilever beams is complex and variable. Therefore, research on the mechanical behavior of the beam not only provides a theoretical basis for the optimization of structural design, but also improves the reliability of structural operation.

Many scholars have analyzed the vibration characteristics of the tapered cantilever beam, Wagner [4] studied the large-amplitude free vibration of the cantilever beam and obtained the nonlinear frequency of the elastic beam under large dynamic deflection. Mabie and Rogers [5] derived the differential equation developed from the Bernoulli-Euler equation for the free vibrations of a double-tapered cantilever beam, and established the table to study the effect of taper ratios on frequency. Nageswara Rao and Venkateswara Rao [6] studied the large amplitude vibration of the free end of the tapered cantilever beam, proposed the corresponding vibration equation and solved the frequency of the beam. Abdel-Jaber *et al.* [7] [8] derived the mathematical model of the beam, and analyzed the nonlinear characteristics of the beam. Al-Raheimy [9] studied the free transverse vibration characteristics of the cantilever beam under the conditions of conical thickness and constant width and conical width and constant width. Wang [10] solved the vibration frequency of an equal-thickness cantilever beam with a linearly tapered width, and analyzed the influence of tip mass, base solidity, and taper on the natural frequency. Baghani *et al.* [11] proposed an efficient and accurate analytical expression for the large amplitude free vibration analysis of single and double tapered beams on elastic foundation, and studied the influence of different parameters on the nonlinear natural frequency of beams under different modal shapes. For the vibration problem of a tapered-shaped cantilever beam, many researchers have proposed many methods that can solve its vibration problems under complex geometrical shapes and various boundary conditions. These solutions have high efficiency and accuracy [12]-[16].

From the above reference, it can be found that many scholars have extensively studied the dynamics of the cantilever beam, exploring the effects of taper, loading conditions, and varying amplitudes through diverse theoretical approaches. However, few scholars have considered the geometrically exact beam theory, which has obvious advantages in dealing with the nonlinear problems of beams. Geometrically exact beam theory, as a beam theory that can efficiently and accurately deal with the large displacement and large rotation of beams, provides a solid theoretical basis for establishing an idealized mathematical model of beams. Geometrically exact beam theory [17]-[23] is a kind of nonlinear beam theory with obvious advantages in dealing with beam structures affected by large displacement and large rotation. This theory is also called Simo-Reissner [17] beam theory. It was first proposed by Reissner [19]-[21], and then developed by Reissner [19], Simo and Vu-Quoc [21] [22] and other pioneers to consider shear and torsional distortion. Many scholars have obtained many research results based on geometrically exact beam theory [24]-[26].

According to the author's knowledge, there is no relevant research on the vibration analysis of the tapered cantilever beam based on geometrically exact beam theory. Therefore, based on the geometrically exact beam theory, combined with virtual displacement principle and d'Alembert principle, the nonlinear dynamic model of the tapered cantilever beam is established. Considering the influence of

shear strain and moment of inertia, the frequency variation of the variable cross-section cantilever beam is studied when the height (width) changes linearly along the axis of the beam. The influence of different taper ratios and slenderness ratios on the frequency of the beam is analyzed. The weak form quadrature element method [27] is used to discretize the dynamic equations. The natural frequency of the cantilever beams is solved and compared with the existing literature to illustrate the effectiveness of the theoretical method. For the vibration analysis of the cantilever beam, the linear frequency and mode of the cantilever beam under different loads, and different bending moments at the free end of the beam are given.

2. Found the Mathematical Model

Considering the length of the cantilever beam is L, the initial centroid axis of the beam coincides with the X-axis of the rectangular coordinate system, as shown in Figure 1.

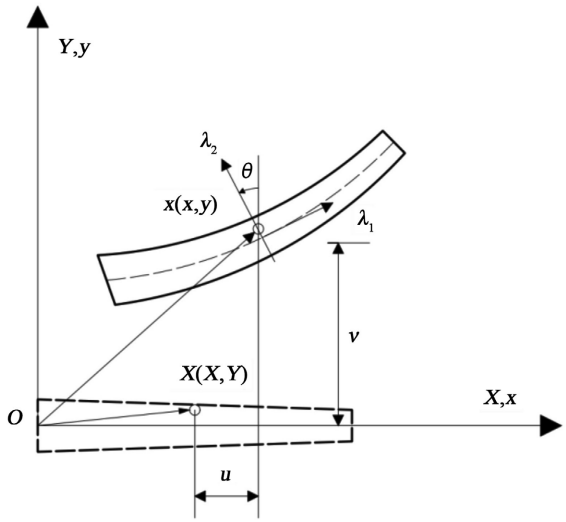

Figure 1. Initial and deformed configurations of the beam.

The u, v, and θ respectively represent axial displacement, transverse displacement, and rotation angle, where u, v and θ are all functions of X. The shape of the beam is represented by displacement vector $\varsigma = (u, v, \theta)^{\mathrm{T}}$. The cross-section direction vectors $\boldsymbol{\lambda}_1$ and $\boldsymbol{\lambda}_2$, which are perpendicular and parallel to the cross-section respectively

$$\boldsymbol{\lambda}_1 = \begin{Bmatrix} \cos\theta \\ \sin\theta \end{Bmatrix} \quad \boldsymbol{\lambda}_2 = \begin{Bmatrix} -\sin\theta \\ \cos\theta \end{Bmatrix} \tag{1}$$

For the beam shown in Figure 2(a), let $\alpha_h = h_l / h_o$, the height, cross-sectional area and moment of inertia at any position of part of the beam can be expressed as follows

$$h_X = h_o - (h_o - h_l) X / L \tag{2a}$$

$$A_X = b h_X \tag{2b}$$

$$I_X = bh_X^3/12 \tag{2c}$$

where h_o is the height of the fixed end of the beam, h_l is the height of the free end of the beam, and b is the width of the beam, h_X is the height of the cross-section at point X, I_X is the moment of inertia the cross-section at point X.

For the beam shown in Figure 2(b), let $\alpha_b = b_l/b_o$, the width, cross-sectional area and moment of inertia at any position of part of the beam can be expressed as follows

$$b_X = b_o - (b_o - b_l)X/L \tag{3a}$$

$$A_X = b_X h \tag{3b}$$

$$I_X = b_X h^3/12 \tag{3c}$$

where b_o is width of the fixed end of the beam, b_l is the height of the free end of the beam, and h is the height of the beam, h_X is the height of the cross-section at point X, I_X is the moment of inertia of the cross-section at point X.

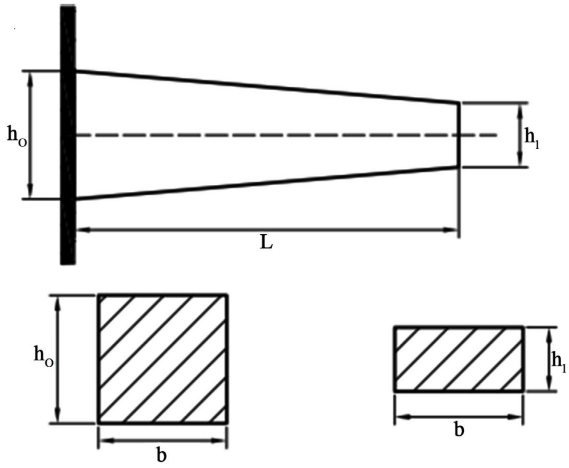

(a) Height changed linearly

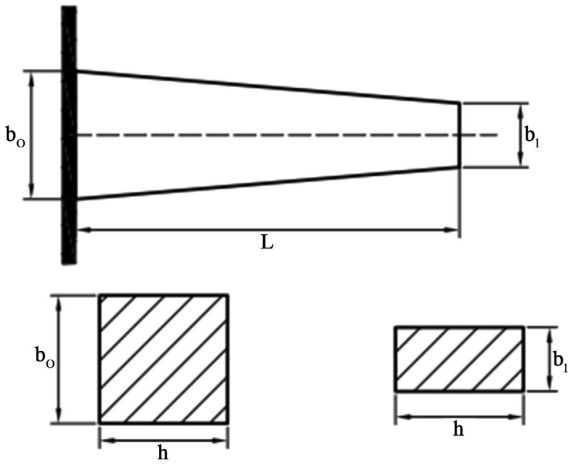

(b) Width changed linearly

Figure 2. Plane diagram of the cantilever beam.

In the Lagrange description, suppose that the position of a point on the beam is $\boldsymbol{X}=(X,Y)^{\mathrm{T}}$ in the initial state, and the position of the point on the current configuration is $\boldsymbol{x}=(x,y)^{\mathrm{T}}$ after deformation. Suppose that the section is not deformed, then the current position vector $\boldsymbol{x}$ can be expressed as follows

$$\boldsymbol{x}=\begin{Bmatrix}x\\y\end{Bmatrix}=\boldsymbol{r}+Y\boldsymbol{\lambda}_2 \quad \boldsymbol{r}=\begin{Bmatrix}X+u\\v\end{Bmatrix} \tag{4}$$

Based on the geometrically exact beam theory, the Reissner strain vector $\boldsymbol{\chi}$ [17]-[19] expressed as follows

$$\boldsymbol{\chi}=\begin{Bmatrix}\varepsilon\\\gamma\\\kappa\end{Bmatrix}=\begin{Bmatrix}\boldsymbol{\lambda}_1^{\mathrm{T}}\boldsymbol{r}'-1\\\boldsymbol{\lambda}_2^{\mathrm{T}}\boldsymbol{r}'\\\theta'\end{Bmatrix} \tag{5}$$

where ε is the corresponding axial strain, γ is the shear strain, κ is the bending strains, $\boldsymbol{r}'$ represents the stretching of the beam axis after deformation, $\boldsymbol{\lambda}_1^{\mathrm{T}}\boldsymbol{r}'$ represents the projection of the stretching of the beam axis in the vertical direction of the section. $\boldsymbol{\lambda}_1^{\mathrm{T}}\boldsymbol{r}'$ represents the projection of the stretching of the beam axis in the horizontal direction of the section. The derivative of $\boldsymbol{\chi}$

$$\delta\boldsymbol{\chi}=\boldsymbol{\Gamma}\begin{Bmatrix}\delta\zeta'\\\delta\theta\end{Bmatrix}=\begin{bmatrix}\boldsymbol{\lambda}_1^{\mathrm{T}} & 0 & \boldsymbol{\lambda}_2^{\mathrm{T}}\boldsymbol{r}'\\\boldsymbol{\lambda}_2^{\mathrm{T}} & 0 & -\boldsymbol{\lambda}_1^{\mathrm{T}}\boldsymbol{r}'\\0_{1\times 2} & 1 & 0\end{bmatrix}\begin{Bmatrix}\delta\boldsymbol{r}'\\\delta\theta'\\\delta\theta\end{Bmatrix} \tag{6}$$

Derived from Reference [28], the equivalent section force is $\boldsymbol{N}_c$, and the constitutive relation matrix is $\boldsymbol{D}_c$

$$\boldsymbol{N}_c=\begin{Bmatrix}N\\V\\M\end{Bmatrix}=\boldsymbol{D}_c\boldsymbol{\chi}=\begin{bmatrix}k_{EA}EA_X & 0 & 0\\0 & k_SGA_X & EB\\0 & EB & k_{EI}EI_X\end{bmatrix}\begin{Bmatrix}\varepsilon\\\gamma\\\kappa\end{Bmatrix} \tag{7}$$

which N, V and M represent the axial force, shear force and bending moment of the section respectively, E and G are Young's modulus and shear modulus respectively. The correction coefficients are obtained from Reference [29]

$$k_{EA}=\left(1-\frac{2}{3}\tau^2\right)\quad k_{EI}=1+\frac{(\mu-48)\mu-45}{45(\mu+1)}\tau^2\quad k_s=\frac{5}{6} \tag{8}$$

where μ is the shear Poisson's ratio.

When the taper angle parameters of the beam with a linear height change and a constant width are

$$\tau=(h_o-h_l)/(2L),\ \ EB=Eb(5\mu+3)h_X^2\tau/(9\mu+9) \tag{9}$$

When the beam with linear width variation and constant height, the taper angle parameters are

$$\tau=(b_o-b_l)/(2L),\ \ EB=Eb_X(5\mu+3)h^2\tau/(9\mu+9) \tag{10}$$

Based on the principle of virtual displacement and D'Alembert's principle, the weak form dynamic equation of the geometrically exact beam expressed as follows

$$\delta W_{int} + \delta W_{ine} - \delta W_{ext} = 0 \tag{11}$$

Then, the whole beam structure is divided into several elements, and defined the dimensionless coordinate $\xi = 2X/L_e - 1$ on $[-1,1]$, where L_e is the length of the beam element. For the beam element, the virtual work of internal force expressed as follows

$$\delta W_{int}^e = \int_0^{L_e} \delta \boldsymbol{\chi}^{\mathrm{T}} \boldsymbol{N}_c \mathrm{d}X = \frac{L_e}{2} \int_{-1}^{1} \delta \boldsymbol{\chi}^{\mathrm{T}} \boldsymbol{N}_c \mathrm{d}\xi \tag{12}$$

where $\delta\boldsymbol{\chi}$ as shown in Equation (6), and $\boldsymbol{N}_c$ as shown in Equation (7).

The virtual work of inertial force of the beam element expressed as follows

$$\delta W_{ine}^e = \int_0^{L_e} \left(\delta \boldsymbol{r}^{\mathrm{T}} \boldsymbol{m}_r \ddot{\boldsymbol{r}} + \delta\theta^{\mathrm{T}} \boldsymbol{J} \ddot{\theta} \right) \mathrm{d}X = \frac{L_e}{2} \int_{-1}^{1} \left(\delta \boldsymbol{r}^{\mathrm{T}} \boldsymbol{m}_r \ddot{\boldsymbol{r}} + \delta\theta^{\mathrm{T}} \boldsymbol{J} \ddot{\theta} \right) \mathrm{d}\xi \tag{13}$$

where $\ddot{\boldsymbol{r}}$ is the acceleration of the centroid of the beam section, $\ddot{\theta}$ is the angular acceleration of the beam section, $\boldsymbol{m}_r$ is the mass of the beam per unit length, $\boldsymbol{J}$ is the moment of the inertia of the section around the central axis, respectively expressed as follows

$$\ddot{\boldsymbol{r}} = \begin{bmatrix} \ddot{u} \\ \ddot{v} \end{bmatrix}, \quad \boldsymbol{m}_r = \begin{bmatrix} \rho A & 0 \\ 0 & \rho A \end{bmatrix}, \quad \boldsymbol{J} = \rho I \tag{14}$$

where $\ddot{u}$ represents the second derivative of axial displacement with respect to time, $\ddot{v}$ represents the second derivative of transverse displacement with respect to time, ρ is the density of the beam, ρ is the cross-sectional area of the beam, and I is the moment of inertia of the cross-section.

The beam element distributed load vector $\boldsymbol{f}$ and the element concentrated load vector $\boldsymbol{F}$ are defined as follows

$$\boldsymbol{f} = \begin{bmatrix} f_P & f_Q & f_M \end{bmatrix}^{\mathrm{T}}, \quad \boldsymbol{F} = \begin{bmatrix} F_P & F_Q & F_M \end{bmatrix}^{\mathrm{T}} \tag{15}$$

The virtual work of external force of the beam element expressed as follows

$$\delta W_{ext}^e = \int_0^{L_e} \delta\varsigma^{\mathrm{T}} \boldsymbol{f} \mathrm{d}X + \delta\varsigma_1^{\mathrm{T}} \boldsymbol{F}_0 + \delta\varsigma_N^{\mathrm{T}} \boldsymbol{F}_L = \frac{L_e}{2} \int_{-1}^{1} \delta\varsigma^{\mathrm{T}} \boldsymbol{f} \mathrm{d}\xi + \delta\varsigma_1^{\mathrm{T}} \boldsymbol{F}_0 + \delta\varsigma_N^{\mathrm{T}} \boldsymbol{F}_L \tag{16}$$

where $\boldsymbol{f}$ is the element distribution load vector, $\boldsymbol{F}_0$ and $\boldsymbol{F}_L$ are from Equation (15), respectively, which represent the concentrated load vectors applied to the fixed end and the free end of the beam.

Substitute Equation (12), Equation (13), and Equation (16) into the Equation (11), the dynamic equation of the geometrically exact beam element states that

$$\begin{aligned} &\frac{L_e}{2} \int_{-1}^{1} \delta \boldsymbol{\chi}^{\mathrm{T}} \boldsymbol{N}_c \mathrm{d}\xi + \frac{L_e}{2} \int_{-1}^{1} \left(\delta \boldsymbol{r}^{\mathrm{T}} \boldsymbol{m}_r \ddot{\boldsymbol{r}} + \delta\theta^{\mathrm{T}} \boldsymbol{J} \ddot{\theta} \right) \mathrm{d}\xi \\ &- \left(\frac{L_e}{2} \int_{-1}^{1} \delta\varsigma^{\mathrm{T}} \boldsymbol{f} \mathrm{d}\xi + \delta\varsigma_1^{\mathrm{T}} \boldsymbol{F}_0 + \delta\varsigma_N^{\mathrm{T}} \boldsymbol{F}_L \right) = \boldsymbol{0} \end{aligned} \tag{17}$$

Using the weak form quadrature element method [27] [30] to discretize Equation (17), we can obtain the following equation

$$\begin{aligned} &\frac{L_e}{2} \sum_{k=1}^{N} w_k \delta \boldsymbol{\chi}_k^{\mathrm{T}} \boldsymbol{N}_{ck} + \frac{L_e}{2} \sum_{k=1}^{N} w_k \left(\delta \boldsymbol{r}_k^{\mathrm{T}} \boldsymbol{m}_{rk} \ddot{\boldsymbol{r}}_k + \delta\theta_k^{\mathrm{T}} \boldsymbol{J}_k \ddot{\theta}_k \right) \\ &- \left(\frac{L_e}{2} \sum_{k=1}^{N} w_k \delta \boldsymbol{\xi}_k^{\mathrm{T}} \boldsymbol{f}_k + \delta\xi_1^{\mathrm{T}} \boldsymbol{F}_0 + \delta\xi_N^{\mathrm{T}} \boldsymbol{F}_L \right) = \boldsymbol{0} \end{aligned} \tag{18}$$

where k is represents the k-th node.

Define the element node displacement vector:

$$\boldsymbol{d}^e = \begin{bmatrix} \boldsymbol{\varsigma}_1^{\mathrm{T}} & \cdots & \boldsymbol{\varsigma}_k^{\mathrm{T}} & \cdots & \boldsymbol{\varsigma}_N^{\mathrm{T}} \end{bmatrix}^{\mathrm{T}}, k = 1, \cdots, N \tag{19}$$

Using the differential quadrature principle from Reference [31] and Equation (6), we obtain $\delta\boldsymbol{\chi}_k$ represented by $\delta\boldsymbol{d}^e$

$$\delta\boldsymbol{\chi}_k = \boldsymbol{\Gamma}_k \begin{Bmatrix} \delta\varsigma_k' \\ \delta\beta_k \end{Bmatrix} = \boldsymbol{\Gamma}_k \boldsymbol{B}_k \delta\boldsymbol{d}^e \tag{20}$$

where $\delta\zeta_k = \boldsymbol{A}_k \delta\boldsymbol{d}^e, \boldsymbol{A}_k = \begin{bmatrix} \delta_{k1}\boldsymbol{I}_{3\times3} & \cdots & \delta_{ki}\boldsymbol{I}_{3\times3} & \cdots & \delta_{kn}\boldsymbol{I}_{3\times3} \end{bmatrix}$, $\boldsymbol{I}$ is identity matrix.

The differential quadrature positioning matrix can be expressed as follows

$$\boldsymbol{B}_k = \begin{bmatrix} \boldsymbol{b}_{k1} & \cdots & \boldsymbol{b}_{ki} & \cdots & \boldsymbol{b}_{kn} \end{bmatrix} \tag{21}$$

where $\boldsymbol{b}_{ki} = \begin{bmatrix} \dfrac{2}{L^e} C_{ki}^{(1)} \boldsymbol{I}_{3\times3} & \boldsymbol{\alpha}_{ki} \end{bmatrix}^{\mathrm{T}}$, $\boldsymbol{\alpha}_{ki} = (0,0,\delta_{ki})$, $\delta_{ki} = \begin{cases} 1, k = i \\ 0, k \neq i \end{cases}$, $C_{ki}^{(1)}$ is first-order differential quadrature weight coefficient from Reference [31].

Substitute Equation (19), Equation (20), and Equation (21) into the Equation (18), we can obtain the dynamic equation

$$\begin{aligned} &\delta\boldsymbol{d}^{e\mathrm{T}} \sum_{k=1}^{N} \frac{L_e}{2} w_k \boldsymbol{B}_k^{\mathrm{T}} \boldsymbol{\Gamma}_k^{\mathrm{T}} \boldsymbol{N}_{ck} + \delta\boldsymbol{d}^{e\mathrm{T}} \sum_{k=1}^{N} \frac{L_e}{2} w_k \boldsymbol{m}_k \ddot{\boldsymbol{d}}^e \\ &- \delta\boldsymbol{d}^{e\mathrm{T}} \left(\sum_{k=1}^{N} \frac{L_e}{2} w_k \boldsymbol{A}_k^{\mathrm{T}} \boldsymbol{f}_k + \boldsymbol{A}_1^{\mathrm{T}} \boldsymbol{F}_0 + \boldsymbol{A}_N^{\mathrm{T}} \boldsymbol{F}_L \right) = \boldsymbol{0} \end{aligned} \tag{22}$$

where $\ddot{\boldsymbol{d}}^e$ is the second derivative of $\boldsymbol{d}^e$ respect to time, $\boldsymbol{m}_k$ is the node mass matrix of the beam element is expressed as

$$\boldsymbol{m}_k = \rho A_X \boldsymbol{E1}_k^{\mathrm{T}} \boldsymbol{E1}_k + \rho A_X \boldsymbol{E2}_k^{\mathrm{T}} \boldsymbol{E2}_k + \rho I_X \boldsymbol{E3}_k^{\mathrm{T}} \boldsymbol{E3}_k \tag{23}$$

where ρ is the density of the beam, $\boldsymbol{E1}$ represents an $N \times 3N$ matrix where the element in the k-th row and the $(3k\text{-}2)$-th column is 1, and all other elements are 0, and $\boldsymbol{E1}_k$ represents the k-th row of $\boldsymbol{E1}$. $\boldsymbol{E2}$ represents an $N \times 3N$ matrix where the element in the k-th row and the $(3k\text{-}1)$-th column is 1, and all other elements are 0, and $\boldsymbol{E2}_k$ represents the k-th row of $\boldsymbol{E2}$. $\boldsymbol{E3}$ represents an $N \times 3N$ matrix where the element in the k-th row and the $3k$-th column is 1, and all other elements are 0, and $\boldsymbol{E3}_k$ represents the k-th row of $\boldsymbol{E3}$.

The mass matrix of beam element can be expressed as follows

$$\boldsymbol{M}_e = \frac{L_e}{2} \sum_{k=1}^{N} w_k \boldsymbol{m}_k, \ k = 1, \cdots, N \tag{24}$$

According to the principle of virtual work, the dynamic equation of the beam element is expressed as follows

$$\delta\boldsymbol{d}^{e\mathrm{T}} \left(\boldsymbol{M}_e \ddot{\boldsymbol{d}}^e + \boldsymbol{R}_{int}^e - \boldsymbol{R}_{ext}^e \right) = \boldsymbol{0} \tag{25}$$

From the independence of the $\delta\boldsymbol{d}^{e\mathrm{T}}$, the equation given as

$$\boldsymbol{M}_e \ddot{\boldsymbol{d}}^e + \boldsymbol{R}_{int}^e - \boldsymbol{R}_{ext}^e + = \boldsymbol{M}_e \ddot{\boldsymbol{d}}^e + \boldsymbol{R} = \boldsymbol{0} \tag{26}$$

For solving the frequency of the beam, the equation needs to be linearized. Without considering the increase of external load, linear increments $\Delta\boldsymbol{R} = \boldsymbol{K}_T \Delta\boldsymbol{d}$

and $\Delta \boldsymbol{R}_{ine} = \boldsymbol{M}\Delta\ddot{\boldsymbol{d}}$ can be obtained. Therefore, the linearized equilibrium equation in the incremental form is as follows

$$\boldsymbol{M}\Delta\ddot{\boldsymbol{d}} + \boldsymbol{K}_T\Delta\boldsymbol{d} = \boldsymbol{0} \tag{27}$$

where $\Delta\ddot{\boldsymbol{d}}$ represents the second-order differential of coordinates to time, and $\boldsymbol{K}_T$ is the overall tangential stiffness matrix.

The tangential stiffness matrix of the element as follows

$$\boldsymbol{K}_T^e = \frac{L_e}{2}\sum_{k=1}^{n} w_k \boldsymbol{B}_k^{\mathrm{T}}\left(\boldsymbol{\Gamma}_k^{\mathrm{T}}\boldsymbol{D}_k\boldsymbol{\Gamma}_k + \boldsymbol{\Xi}_k\right)\boldsymbol{B}_k \tag{28}$$

where $\boldsymbol{\Xi}_k$ is:

$$\boldsymbol{\Xi}_k = \begin{bmatrix} 0_{2\times 2} & 0_{2\times 1} & -V_k\lambda_{1k} + N_k\lambda_{2k} \\ 0_{1\times 2} & 0 & 0 \\ -V_k\lambda_{1k}^{\mathrm{T}} + N_k\lambda_{2k}^{\mathrm{T}} & 0 & -N_k\lambda_{1k}^{\mathrm{T}}\boldsymbol{r}_k' - V_k\lambda_{2k}^{\mathrm{T}}\boldsymbol{r}_k' \end{bmatrix} \tag{29}$$

All the global matrices can be obtained by assembling element matrix mentioned above. For the internal nodes of the element, the corresponding component of $\boldsymbol{K}_T$ is equal to the component of $\boldsymbol{K}_T^e$. For the end point of the unit, the corresponding component of $\boldsymbol{K}_T$ is equal to the sum of the $\boldsymbol{K}_T^e$ corresponding components of all the units connected at this point. The total mass matrix $\boldsymbol{M}$ can also be obtained by assembling $\boldsymbol{M}_e$ in this way.

For the linear problem, let the initial displacement vector be $\boldsymbol{d} = \boldsymbol{0}$, the obtained tangential stiffness matrix is a general stiffness matrix, and the result after one iteration is the solution of the linear problem. When the structure is in equilibrium, the equation of state is as follows

$$\boldsymbol{d} = \begin{bmatrix} \varsigma_1 \\ \vdots \\ \varsigma_N \end{bmatrix},\ \boldsymbol{d}_1 = \dot{\boldsymbol{d}},\ \begin{bmatrix} \dot{\boldsymbol{d}} \\ \dot{\boldsymbol{d}}_1 \end{bmatrix} = \begin{bmatrix} \boldsymbol{0} & E \\ \left(-\boldsymbol{M}\right)^{-1}\boldsymbol{K}_T & \boldsymbol{0} \end{bmatrix}\begin{bmatrix} \boldsymbol{d} \\ \boldsymbol{d}_1 \end{bmatrix} \tag{30}$$

the natural frequency can be obtained by solving the state equation.

The following dimensionless parameters are introduced for convenience

$$\omega = \sqrt{\frac{\rho A_l L^4 \psi^2}{EI_l}},\ r_o = \sqrt{\frac{I_o}{A_o}},\ \bar{\boldsymbol{x}} = \frac{\boldsymbol{x}}{L},\ M = \frac{F_M L}{2\pi EI_l},\ Q = \frac{F_Q L^2}{EI_l} \tag{31}$$

where A_l is the cross-sectional area at the free end, I_l is the moment of inertia at the free end, A_o is the cross-sectional area at the free end, I_o is the moment of inertia at the free end.

3. Numerical Results and Discussion

This paper uses two units for numerical calculation, each unit contains 11 nodes to ensure the accuracy of numerical calculation results. The Young's modulus of the beams used in all numerical examples are $E = 720$ Gpa, the Poisson's ratio is $\mu = 0.3$, and the density of the beam are $\rho = 7800\ \mathrm{kg/m^3}$.

Based on the mathematical model of the tapered cantilever beam, the natural frequencies of the beam with the slenderness ratio $L_r = L/r_o = 100$ are obtained by the numerical calculations. The first three frequencies for varied taper ratios are

shown in Table 1.

Table 1. Natural frequencies of the tapered cantilever beam.

		First frequency			Second frequency			Third frequency		
	α_b	Ref [5]	Present work	Error (%)	Ref [5]	Present work	Error (%)	Ref [5]	Present work	Error (%)
$\alpha_h = 1.$	1.0	3.5160	3.5154	0.17	22.035	22.0070	0.13	61.70	61.5140	0.30
	0.5	4.3152	4.3143	0.21	23.519	23.4898	0.12	63.20	63.0108	0.30
	0.2	5.3977	5.3963	0.26	25.656	25.6226	0.13	67.54	65.5474	3.04
$\alpha_h = 0.$	1.0	7.6469	7.6417	0.68	36.632	36.6110	0.06	94.52	94.3768	0.15
	0.5	9.2495	9.2496	0.00	39.092	39.0702	0.06	97.14	97.0009	0.14
	0.2	11.4291	11.4288	0.00	42.700	42.6744	0.06	101.36	101.2169	0.14
$\alpha_h = 0.$	1.0	21.4573	21.4616	0.02	78.682	78.6852	0.00	184.33	184.2551	0.04
	0.5	25.5096	25.5146	0.02	83.973	83.9747	0.00	190.11	190.0158	0.05
	0.2	30.9770	30.9802	0.01	91.895	91.8940	0.00	199.09	198.9875	0.05

Due to space limitations, this paper chooses part of the data to compare with Reference [5]. By comparing the numerical results in Table 1, it can be seen that the maximum relative error between the numerical results obtained and those in Reference [5] is less than 3.5%, not only which proves the correctness of the model, but also demonstrated the efficiency of the model, which can ensure the calculation accuracy while selecting fewer parameters.

From Figure 3, it can be found that for the same values of the taper ratio, the natural frequencies of the beam increase as the slenderness ratio increases. At the same L_r, the frequencies increase with the increase in the taper ratio. The first mode frequency shows little variation with the α_h, while the second and third mode frequencies exhibit more noticeable changes. Notably, when the $L_r > 25$, its impact on the natural frequencies becomes minimal.

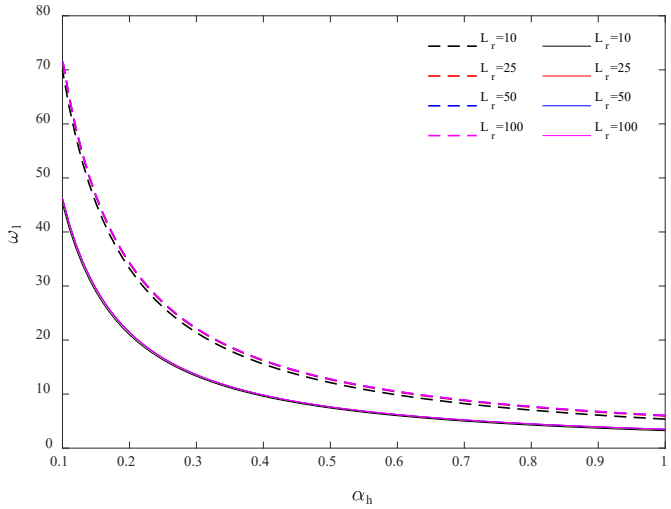

(a) First-order frequency

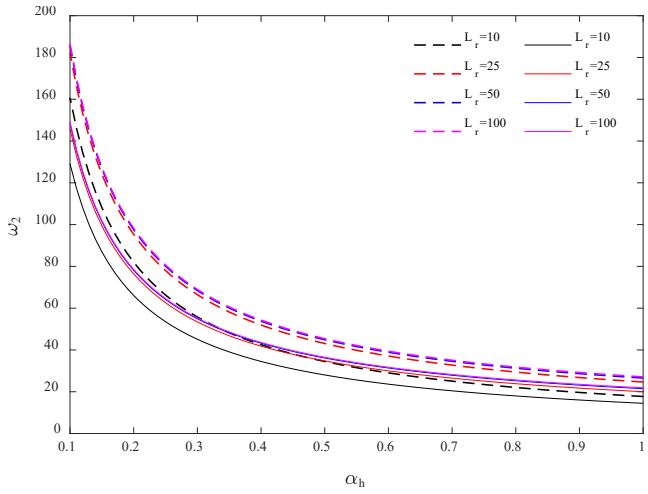

(b) Second-order frequency

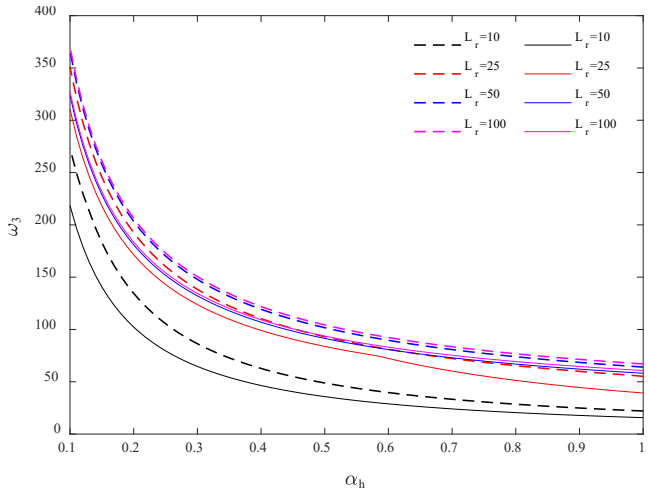

(c) Third-order frequency

Figure 3. The first three natural frequencies of the beam with vary taper ratio, solid line represents $\alpha_b = 0.1$, dashed line represents $\alpha_b = 1$.

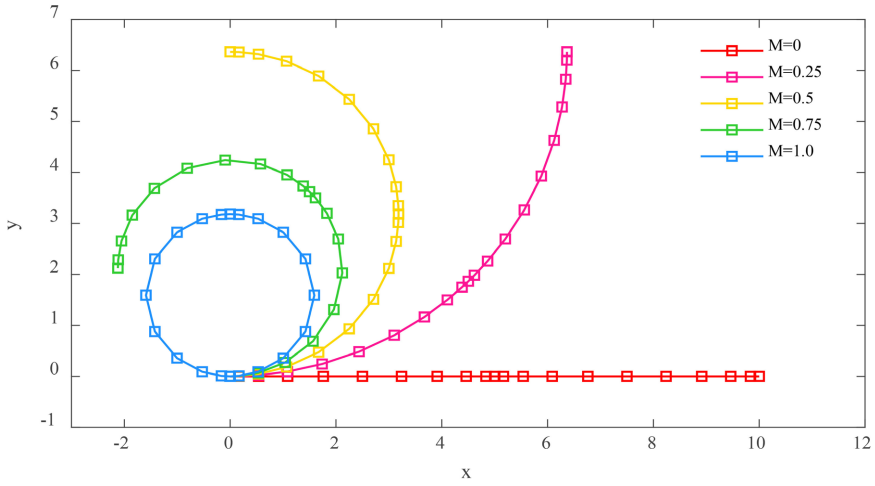

Figure 4. The deformation configuration diagram of the cantilevered beam.

Figure 4 shows that the deformation configuration diagram of the beam under the action of a dimensionless bending moment when $\alpha_h = 1.0$, $\alpha_b = 1.0$ and $L_r = 15$. Comparing the data in Figure 4 with that from Reference [29] verifies that the correctness of the cantilever beam model under the action of the load.

From Table 2, it can be found that when the free end of the beam is subjected to the same dimensionless bending moment, the first three frequencies of the beam increase with the taper ratio. The frequency variation is more significant for the height taper ratio than for the width taper ratio. When the taper ratio is the same, the frequencies of the beam increase as the bending moment at the free end increases.

Table 2. Frequencies of the tapered cantilever beam with an end torque at vary taper ratio.

		$M = 0.5$			$M = 1.0$		
	α_b	ω_1	ω_2	ω_3	ω_1	ω_2	ω_3
$\alpha_h = 1.0$	1.0	4.2909	13.4701	45.5735	7.5797	12.3882	27.1590
	0.5	4.7000	17.9835	55.2122	6.0567	14.1787	42.0872
	0.1	6.1006	26.6177	66.4940	6.2182	25.3815	65.0183
$\alpha_h = 0.5$	1.0	7.8123	33.8417	91.2561	8.3262	29.1235	84.7660
	0.5	9.3484	37.7692	94.9692	9.6545	35.0479	91.4079
	0.1	12.7977	45.3293	104.1842	12.8366	45.1562	103.7606
$\alpha_h = 0.1$	1.0	46.4775	149.9264	328.5651	46.4889	149.9439	328.5319
	0.5	54.6250	159.6463	338.9920	54.6346	159.6777	339.0139
	0.1	72.0465	186.6498	370.2163	72.0487	186.6694	370.2977

The first three transverse modes of the beam under the different taper ratios when $M = 0.50$, $L_r = 15$ and $\alpha_b = 1.0$ are shown in Figure 5.

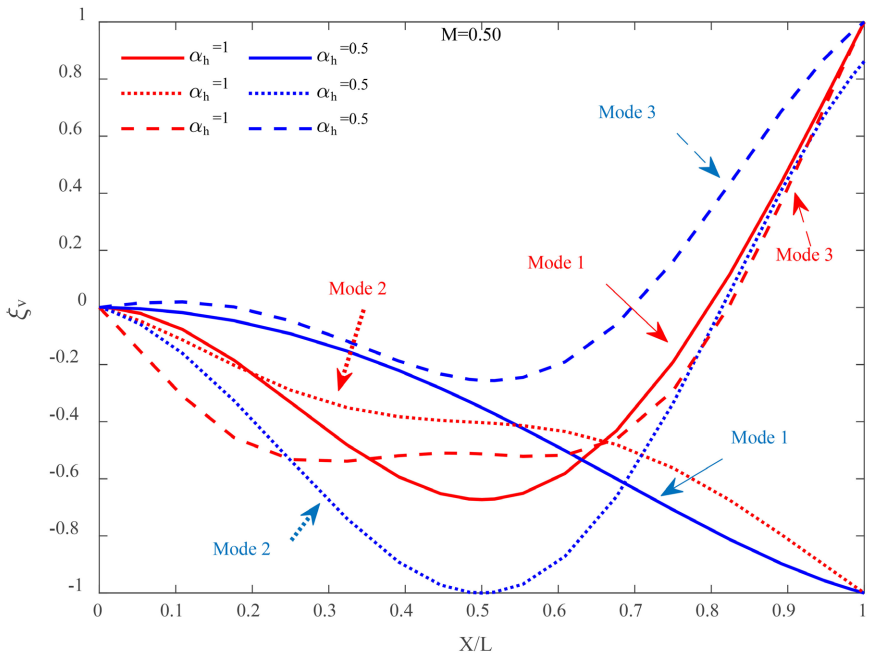

Figure 5. The first three transverse modes of the tapered cantilever beam when $M = 0.05$, $L_r = 15$ and $\alpha_b = 1.0$.

Figure 6 shows the displacement-load curve of the beam under the action of a transverse force at the free end when $\alpha_b = 1.0$ and $L_r = 15$.

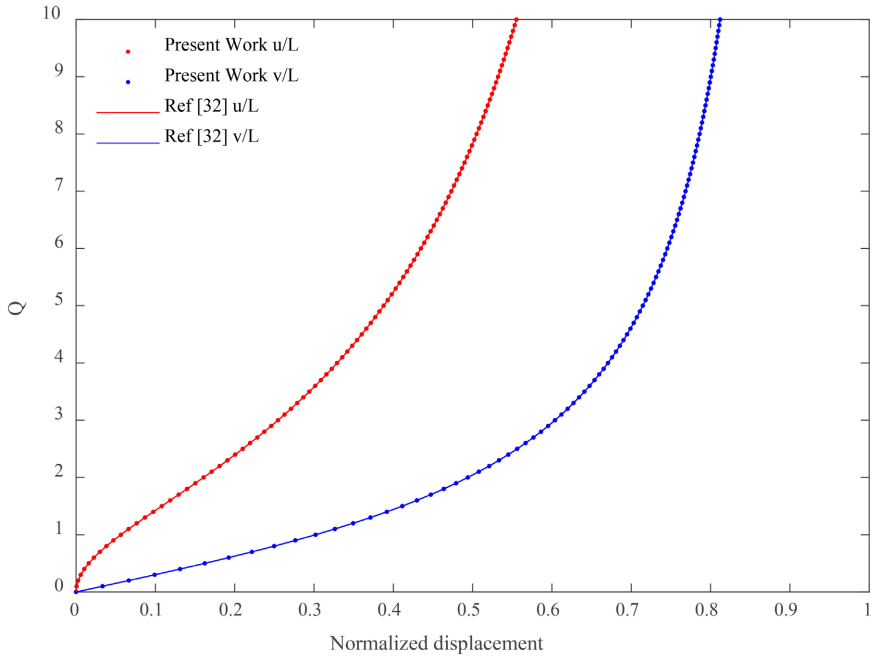

Figure 6. Displacements of the cantilever beam with a tip force.

From Table 3, it can be found that when the free end of the tapered cantilever beam is subjected to the same dimensionless tip force, the first three frequencies of the beam increase with the taper ratio. The frequency variation is more significant for the height taper ratio than for the width taper ratio. When the taper ratio is the same, the frequencies of the beam increase as the tip force at the free end increases.

Table 3. Frequencies of the tapered cantilever beam with a tip force at vary taper ratio.

		$Q = 2.0$			$Q = 10.0$		
	α_b	ω_1	ω_2	ω_3	ω_1	ω_2	ω_3
$\alpha_h = 1.0$	1.0	4.2681	21.2361	57.5136	7.1911	23.2032	55.7280
	0.5	4.7198	23.1183	61.1726	7.1736	23.9482	59.3031
	0.1	6.1017	27.1116	66.9963	6.7926	27.3135	66.8312
$\alpha_h = 0.5$	1.0	7.7676	36.4492	93.5793	9.4152	36.2363	92.3561
	0.5	9.3064	38.9609	96.3218	10.3346	39.0826	96.3082
	0.1	12.8052	45.4247	104.3674	12.9347	45.5605	104.5289
$\alpha_h = 0.1$	1.0	46.2998	149.0949	327.1543	46.3101	149.1161	327.1827
	0.5	54.5022	159.0421	337.9115	54.5086	159.0588	337.9327
	0.1	72.0262	186.5087	369.8805	72.0271	186.5130	369.8875

The first three transverse modes of the beam under the different taper ratios when $Q = 2$, $L_r = 15$ and $\alpha_b = 1.0$ are shown in Figure 7.

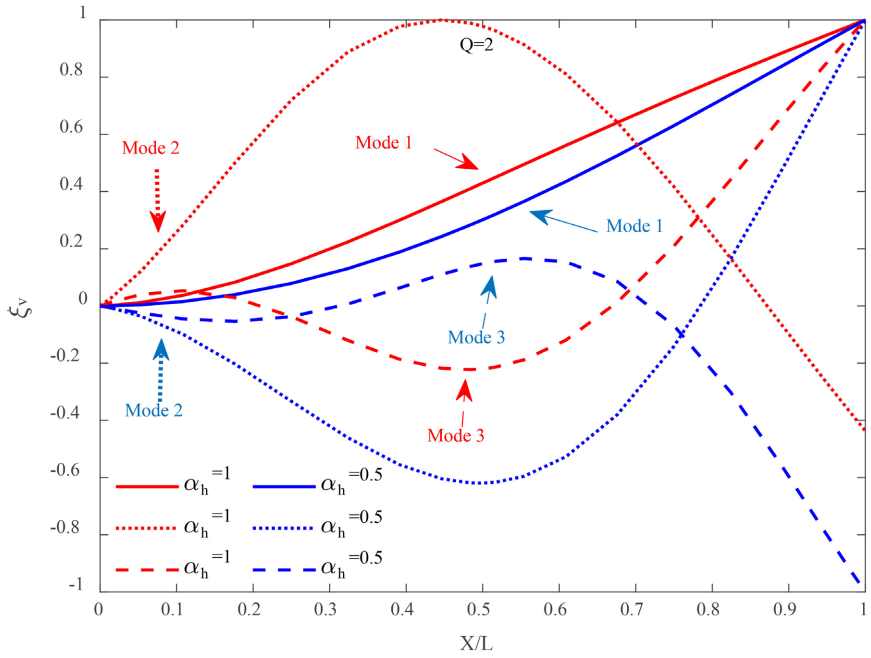

Figure 7. The first three transverse modes of the tapered cantilever beam when $Q=2$, $L_r=15$ and $\alpha_b=1.0$.

4. Conclusions

Based on the theory of geometrically exact beams, this study establishes a mathematical model for the tapered cantilever beam and analyzes the free vibration of the beam. According to the numerical simulation results, the analysis results of the free vibration of the tapered cantilever beam are as follows:

1) Without loading, the natural frequencies of the tapered cantilever beam decrease with an increasing taper ratio, with height taper variation exerting a more pronounced influence on the natural frequency compared to width taper variation.

2) For the same taper ratios and slenderness ratios, the first, second, and third-order frequencies of the beam increase with an increase in amplitude. Similarly, for constant taper ratios, the first three frequencies of the beam increase with an increase in slenderness ratio.

3) When the tapered cantilever beam is subjected to the same dimensionless bending moment, the first three frequencies of the beam increase with the taper ratio. The frequency variation is more significant for the height taper ratio than for the width taper ratio. When the taper ratio is the same, the frequency of the beam increases as the bending moment at the free end increases.

4) When subjected to dimensionless tip force, the first three frequencies of the beam increase with the taper ratio. The frequency variation is more significant for the height taper ratio than for the width taper ratio. When the taper ratio is the same, the frequencies of the beam increase as the tip force at the free end increases.

The geometrically exact beam theory is the beam theory that can efficiently handle large deformations and large displacements of structures. This paper establishes

a mathematical model of the tapered cantilever beam based on the geometrically exact beam theory and analyzes the linear vibration of the structure. In the future, considering the actual working conditions of the structure, we will conduct research on the nonlinear aspects of the structure, thereby being able to describe the mechanical behavior of the structure more accurately, and provide a more comprehensive theoretical basis for the structural reliability and optimization design.

Conflicts of Interest

The authors declare no conflicts of interest regarding the publication of this paper.

References

[1] Todorovska, M.I., Girmay, E.A., Wang, F. and Rahmani, M. (2021) Wave Propagation in a Doubly Tapered Shear Beam: Model and Application to a Pyramid-Shaped Skyscraper. *Earthquake Engineering & Structural Dynamics*, **51**, 764-792. https://doi.org/10.1002/eqe.3590

[2] Gugulothu, S., Kumar, G., Kundu, S., Nemade, H.B. and Trivedi, G. (2017) Design of a Next Generation Framework for MEMS Devices. 2017 *Devices for Integrated Circuit* (*DevIC*), Kalyani, 23-24 March 2017, 546-550. https://doi.org/10.1109/devic.2017.8074010

[3] Campos, L.M.B.C. and Marta, A.C. (2021) On the Vibrations of Pyramidal Beams with Rectangular Cross-Section and Application to Unswept Wings. *The Quarterly Journal of Mechanics and Applied Mathematics*, **74**, 1-31. https://doi.org/10.1093/qjmam/hbaa017

[4] Wagner, H. (1965) Large-Amplitude Free Vibrations of a Beam. *Journal of Applied Mechanics*, **32**, 887-892. https://doi.org/10.1115/1.3627331

[5] Mabie, H.H. and Rogers, C.B. (1972) Transverse Vibrations of Double-Tapered Cantilever Beams. *The Journal of the Acoustical Society of America*, **51**, 1771-1774. https://doi.org/10.1121/1.1913028

[6] Nageswara Rao, B. and Venkateswara Rao, G. (1988) Large Amplitude Vibrations of a Tapered Cantilever Beam. *Journal of Sound and Vibration*, **127**, 173-178. https://doi.org/10.1016/0022-460x(88)90357-4

[7] Abdel-Jaber, M.S., Al-Qaisia, A.A., Abdel-Jaber, M. and Beale, R.G. (2008) Nonlinear Natural Frequencies of an Elastically Restrained Tapered Beam. *Journal of Sound and Vibration*, **313**, 772-783. https://doi.org/10.1016/j.jsv.2007.11.050

[8] Abdel-Jaber, M., Al-Qaisia, A.A. and Abdel-Jaber, M.S. (2009) Nonlinear Natural Frequencies of a Cantilever with Variable Cross-Section Beam. *Advanced Steel Construction*, **5**, 259-272.

[9] Al-Raheimy, N.H. (2013) Transverse Free Vibrations of Tapered Cantilever Beam. *The Iraqi Journal for Mechanical and Material Engineering*, **13**, 254-269.

[10] Wang, C.Y. (2012) Vibration of a Tapered Cantilever of Constant Thickness and Linearly Tapered Width. *Archive of Applied Mechanics*, **83**, 171-176. https://doi.org/10.1007/s00419-012-0637-1

[11] Baghani, M., Mazaheri, H. and Salarieh, H. (2014) Analysis of Large Amplitude Free Vibrations of Clamped Tapered Beams on a Nonlinear Elastic Foundation. *Applied Mathematical Modelling*, **38**, 1176-1186. https://doi.org/10.1016/j.apm.2013.06.040

[12] Keshmiri, A., Wu, N. and Wang, Q. (2018) Free Vibration Analysis of a Nonlinearly Tapered Cone Beam by Adomian Decomposition Method. *International Journal of*

Structural Stability and Dynamics, **18**, Article ID: 1850101. https://doi.org/10.1142/s0219455418501018

[13] Bayat, M., Pakar, I. and Bayat, M. (2011) Analytical Study on the Vibration Frequencies of Tapered Beams. *Latin American Journal of Solids and Structures*, **8**, 149-162. https://doi.org/10.1590/s1679-78252011000200003

[14] Sedighi, H.M., Shirazi, K.H. and Noghrehabadi, A. (2012) Application of Recent Powerful Analytical Approaches on the Non-Linear Vibration of Cantilever Beams. *International Journal of Nonlinear Sciences and Numerical Simulation*, **13**, 487-494. https://doi.org/10.1515/ijnsns-2012-0030

[15] Al-Ansari, L.S., Al-Hajjar, A.M.H. and Jawad, H. (2018) Calculating the Natural Frequency of Cantilever Tapered Beam Using Classical Rayleigh, Modified Rayleigh and Finite Element Methods. *International Journal of Engineering & Technology*, **7**, 4866-4872.

[16] Tang, S. and Sweetman, B. (2019) A Geometrically-Exact Momentum-Based Non-Linear Theory Applicable to Beams in Non-Inertial Frames. *International Journal of Non-Linear Mechanics*, **113**, 158-170. https://doi.org/10.1016/j.ijnonlinmec.2019.03.007

[17] Reissner, E. (1972) On One-Dimensional Finite-Strain Beam Theory: The Plane Problem. *Zeitschrift für Angewandte Mathematik und Physik ZAMP*, **23**, 795-804. https://doi.org/10.1007/bf01602645

[18] Reissner, E. (1973) On One-Dimensional Large-Displacement Finite-Strain Beam Theory. *Studies in Applied Mathematics*, **52**, 87-95. https://doi.org/10.1002/sapm197352287

[19] Reissner, E. (1981) On Finite Deformations of Space-Curved Beams. *Zeitschrift für Angewandte Mathematik und Physik ZAMP*, **32**, 734-744. https://doi.org/10.1007/bf00946983

[20] Simo, J.C. (1985) A Finite Strain Beam Formulation. the Three-Dimensional Dynamic Problem. Part I. *Computer Methods in Applied Mechanics and Engineering*, **49**, 55-70. https://doi.org/10.1016/0045-7825(85)90050-7

[21] Simo, J.C. and Vu-Quoc, L. (1986) A Three-Dimensional Finite-Strain Rod Model. Part II: Computational Aspects. *Computer Methods in Applied Mechanics and Engineering*, **58**, 79-116. https://doi.org/10.1016/0045-7825(86)90079-4

[22] Simo, J.C. and Vu-Quoc, L. (1991) A Geometrically-Exact Rod Model Incorporating Shear and Torsion-Warping Deformation. *International Journal of Solids and Structures*, **27**, 371-393. https://doi.org/10.1016/0020-7683(91)90089-x

[23] Vu-Quoc, L. and Li, S. (1995) Dynamics of Sliding Geometrically-Exact Beams: Large Angle Maneuver and Parametric Resonance. *Computer Methods in Applied Mechanics and Engineering*, **120**, 65-118. https://doi.org/10.1016/0045-7825(94)00051-n

[24] Wang, L., Liu, X., Renevier, N., Stables, M. and Hall, G.M. (2014) Nonlinear Aeroelastic Modelling for Wind Turbine Blades Based on Blade Element Momentum Theory and Geometrically Exact Beam Theory. *Energy*, **76**, 487-501. https://doi.org/10.1016/j.energy.2014.08.046

[25] Invernizzi, D. and Dozio, L. (2016) A Fully Consistent Linearized Model for Vibration Analysis of Rotating Beams in the Framework of Geometrically Exact Theory. *Journal of Sound and Vibration*, **370**, 351-371. https://doi.org/10.1016/j.jsv.2016.01.049

[26] Chadha, M. and Todd, M.D. (2020) The Mathematical Theory of a Higher-Order Geometrically-Exact Beam with a Deforming Cross-Section. *International Journal of Solids and Structures*, **202**, 854-880. https://doi.org/10.1016/j.ijsolstr.2020.06.002

[27] Zhong, H. and Yu, T. (2006) Flexural Vibration Analysis of an Eccentric Annular Mindlin

Plate. *Archive of Applied Mechanics*, **77**, 185-195. https://doi.org/10.1007/s00419-006-0083-z

[28] Xiao, N. and Zhong, H. (2012) Non-linear Quadrature Element Analysis of Planar Frames Based on Geometrically Exact Beam Theory. *International Journal of Non-Linear Mechanics*, **47**, 481-488. https://doi.org/10.1016/j.ijnonlinmec.2011.09.021

[29] Hodges, D., Rajagopal, A., Ho, J. and Yu, W. (2010) Stress and Strain Recovery for the In-Plane Deformation of an Isotropic Tapered Strip-Beam. *Journal of Mechanics of Materials and Structures*, **5**, 963-975. https://doi.org/10.2140/jomms.2010.5.963

[30] Conway, H.D., Becker, E.C.H. and Dubil, J.F. (1964) Vibration Frequencies of Tapered Bars and Circular Plates. *Journal of Applied Mechanics*, **31**, 329-331. https://doi.org/10.1115/1.3629606

[31] Bellman, R. and Casti, J. (1971) Differential Quadrature and Long-Term Integration. *Journal of Mathematical Analysis and Applications*, **34**, 235-238. https://doi.org/10.1016/0022-247x(71)90110-7